A Hybrid Active-Passive Actuation and Control Approach for Kinesthetic Handheld Haptics

Patrick Dills, Nick Colonnese, Priyanshu Agarwal, Michael Zinn, *Member, IEEE*

***Abstract*— Handheld haptic devices are often limited in rendering capability, as compared to traditional grounded devices. Strenuous design criteria on weight, size, power consumption, and the ungrounded nature of handheld devices, can drive designers to prioritize actuator force or torque production over other components of dynamic range like bandwidth and transparency. Hybrid actuation, the use of passive and active actuators together, has the potential to increase the dynamic range of handheld haptic devices due to the large passive torque capability of passive actuators, the high bandwidth of conventional DC servomotors, and the synergy between them. However, to date the use of hybrid actuation has been limited due to the highly nonlinear torque characteristics of available passive actuators that result in poor rendering accuracy. This paper describes a novel hybrid actuation approach and control topology, which aims to solve actuation challenges in hybrid and handheld haptic devices. The performance of the device is assessed experimentally, and the approach is compared to existing handheld devices.**

I. Introduction

Actuators for grounded kinesthetic haptic devices have been a focus of research for many years. However, new developments in augmented and virtual reality have opened a new area of haptics research focusing on ungrounded handheld and wearable haptic devices. Traditional grounded kinesthetic haptic device design criteria, composing dynamic range, still apply to this new generation of devices. The mobile nature of these new ungrounded devices impose additional and more strenuous size and weight requirements than traditional grounded kinesthetic devices. As a result, actuation approaches used in these devices often address only a subset of the total actuation requirements. New hybrid actuators, the combination of active and passive actuators, has the potential to fully address actuation design requirements of ungrounded handheld haptic devices.

Typical kinesthetic actuation approaches used in existing ungrounded handheld and wearable devices have adopted various design approaches. While somewhat subjective, we have organized this prior work into five categories, classified according to the type and characteristics of the actuation approach used (see Table 1).

The first actuation category is comprised of passive and shape rendering devices that utilize mechanical brakes to render kinesthetic feedback to the user. Actuation approaches in this class of device take the form of a brake which can be used to render the shape of the virtual object or a limited set of virtual impedances [1,2]. These devices can typically provide very large forces, due to their passive shape rendering mechanisms, but lack the ability to render a diverse range of impedances.

The second actuation category includes devices that utilize highly-geared electric motors, providing a high force/torque density while minimizing weight and resource usage. These devices incorporate output force or torque sensing for feedback and are controlled in an admittance mode where a force control loop is wrapped around the position control loop to render the virtual environment [3]. These actuators are limited by their position control bandwidth and consequently are limited in transparency and force bandwidth.

The third actuation category consists of devices that utilize compliant actuation, typically controlled as a series elastic actuator (SEA) [4]. This approach has been adopted for wearable hand exoskeletons [5,6]. These actuators place a compliant (series elastic) element between the user and the actuator, allowing for closed loop force control through the measurement of the compliant element's deflection. Speed reducers used in the SEA increase the range of controllable force magnitudes while maintaining transparency, but they are limited in force control bandwidth.

The fourth actuation category consists of devices that pair electric motors with a small speed reducer, (e.g. planetary or cable reduction) and are often used to provide kinesthetic feedback in hand-centered haptic devices [7,8]. This approach can provide larger forces and torques but can reduce device transparency if reduction ratios are large.

The final actuation category consists of devices that use pneumatic actuators. These devices can address force magnitude and transparency requirements but have trouble providing the torque bandwidth needed for a high-quality rendering [8,9]. Table 1 summarizes which high-level ungrounded kinesthetic haptic design requirements are addressed by each of the five actuation categories discussed.

TABLE I. Actuation Approaches Common to Handheld Kinesthetic Haptic Devices

Actuation Approach	Kinesthetic Haptics Design Criteria: Composing Dynamic Range				
	Large Forces	*Large Bandwidth of Force*	*Transparent*	*High Stiffness*	*Variable Impedance Rendering*
Brakes or Shape Rendering [1,2]	✓	✗	✓	✓	✗
Admittance Control Devices [3]	✓	✗	✗	✓	✓
Series Elastic Actuatior Devices [5,6]	✓	✗	✓	✗	✓
Geared DC Motors [7,8]	✓	✓	✗	✓	✓
Pnumatic and Soft Actuators [8,9]	✓	✗	✓	✗	✓

Patrick Dills and Michael Zinn are with the Department of Mechanical Engineering at the University of Wisconsin-Madison. (e-mail: pdills|mzinn@wisc.edu). Nick Colonnese and Priyanshu Agarwal are with Facebook Reality Labs.

Hybrid actuation has been shown to increase the stable range of rendered impedances, increase torque density, and improve energy efficiency as compared to active-only solutions in grounded impedance-based kinesthetic haptic devices [10-12] and can provide variable impedance rendering that passive-only approaches do not. While hybrid actuation appears to be a promising approach, the highly nonlinear torque characteristics of currently available passive actuation, particularly acute during velocity reversals, has made it challenging to create accurate haptic effects. As such, hybrid actuators have not been widely adopted by grounded kinesthetic haptic displays and have never, to our knowledge, been incorporated into an ungrounded handheld device.

To mitigate the nonlinear characteristics of available passive actuation while maintaining its beneficial characteristics, including energy dissipation and high static load capability, various control and mechanical design approaches have been investigated. Control approaches have included techniques to reduce the passive actuator's effect at low velocity and thus eliminate the rapid and difficult to predict torque fluctuations that can occur [13,14]. While effective in increasing rendering accuracy, the beneficial high-static torque available is reduced significantly. Mechanical solutions have relied on complex mechanical components to address the undesirable nonlinear characteristics typical of passive actuators, complicating the mechanical design and increasing weight. Examples of this include designs that incorporate multiple brakes and overrunning clutches [15], a mechanical differential [16], and springs [12] to maintain transparency and improve performance. Actuation approaches with complicated mechanical designs are generally excluded from consideration due to the size and weight constraints of handheld haptic devices. In summary, existing hybrid actuation methods have failed to address the full range of design requirements of high-performance handheld kinesthetic haptic interfaces.

To mitigate the undesirable nonlinear characteristics of passive actuators and realize benefits of hybrid actuation, including increased rendering range or Z-width, we have developed a new hybrid actuation approach for handheld haptic devices, conceptually shown in Fig. 1. Our approach seeks to address hybrid design and control challenges with a novel passive torque partitioning method and control structure which enables simple mechanical design required in lightweight handheld haptic devices.

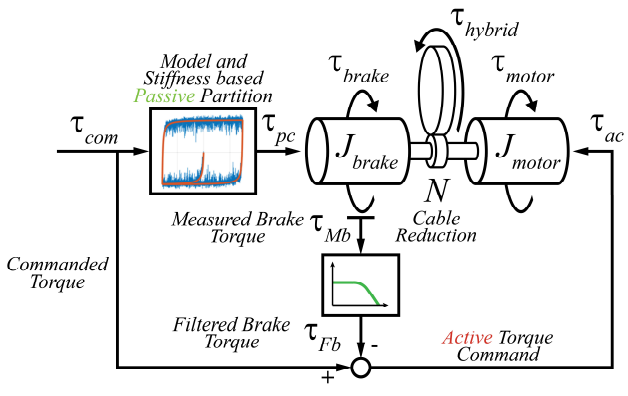

Figure 1. Hybrid actuation approach model and signal flow diagram.

The passive actuator partitioning method employs an accurate passive actuator torque model to partition desired actuation torques according to the constrained dynamics of the passive actuator, isolating torque components that can be rendered by the passive actuator while shunting the remaining torque components to the active actuator. This model-based approach significantly improves passive torque partitioning when compared to existing methods, largely eliminating the nonlinear switching behavior common to simple partitioning approaches based on power flow [13,15]. In addition to model-based partitioning, active feedback of passive actuator error allows the active actuator to compensate for the remaining undesirable nonlinear passive actuator torques causing rendering errors and to maintain transparency. Our hybrid actuation approach achieves a larger dynamic range than each component individually while virtually eliminating rendering distortion. Finally, our control method enables a simple low impedance mechanical design necessary to bring hybrid actuation to the handheld form factor. The handheld hybrid actuation approach presented here fulfills the design requirements identified as important to kinesthetic haptic actuators while satisfying additional size and weight requirements imposed by the handheld haptic format.

The discussion and evaluation of our proposed handheld hybrid actuation approach are organized into three sections. The first section focuses on hybrid actuation control challenges and how they are resolved by our control approach. A discussion of mechanical design elements critical to hybrid handheld haptic device performance constitutes the second section. Finally, the performance of our prototype device is experimentally evaluated and compared to existing haptic devices from each category.

I. Hybrid Actuator Control

A fundamental function of a hybrid actuators control system is to partition a desired torque command into commands for each actuator. This partitioning effectively creates a single input single output system (SISO) from a dual input single output device (DISO) as seen in Fig. 2. The challenge and goal of hybrid control is to partition torques in a way which improves dynamic range and does not impact the haptic rendering.

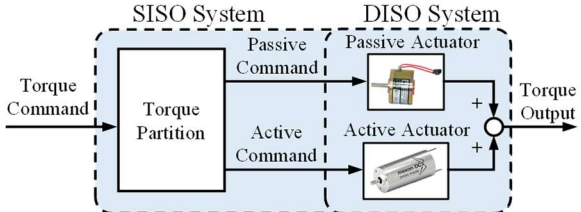

Figure 2. Generalized control topology of a multi-input single output hybrid actuator recast into a single input single output system.

Methods to achieve this goal are varied and include partitioning approaches based on power flow [13,15], the rendered impedance where the passive actuator renders damping torques while the active actuator supplies stiffness torques [10], and by measuring the deflection of a series elastic spring to estimate brake torque production and partitioning the active torque accordingly [12]. Additional torque partitioning methods utilize: a first order transfer function to partition the passive and active torque [14], an active actuator as a velocity

source and the brake as a torque source [16], and a passivity observer and controller to generate brake commands [17]. Experimentation with our hybrid system has revealed that the torque partitioning approach has significant impact on the devices rendering quality, performance, and rendering range.

Our goals for our hybrid control approach are three-fold. Our hybrid control approach should meet or exceed the dynamic range of a typical active only impedance based haptic device utilizing a DC motor. Our control system should solve control challenges common to hybrid devices like the "sticky wall" effect [13,14] while taking advantage of zero velocity passive torque produced by brakes. Finally, because of size and weight restrictions on handheld haptic devices, our control approach should remove the need for additional mechanical components such as clutches and differentials to achieve a quality rendering.

Fig. 1 shows the general control approach for our handheld hybrid haptic device. Initially, the torque command is fed through a dynamic model of the passive actuator (to be described in more detail in the next section) from which the passive actuator commanded torque is developed. This step is referred to as passive partitioning. The difference between the measured passive actuator torque and the total torque command is used to form the active actuator's torque command. Measured torque feedback allows the high bandwidth servo motor to compensate for unwanted passive torques and to produce torque the passive actuator cannot.

A. *Particle Brake Dynamics*

An essential part of our proposed model-based passive actuator partitioning approach is the development of an accurate passive actuator physical model. To motivate our modeling approach, it is instructive to discuss the specifics of the passive actuator's design. In our work, we have used a particle brake, which can produce controllable passive torques when current is passed through a coil generating an electromagnetic field. The field binds the rotor and stator together via ferrous metal particles and resulting torques resist motion of the rotor. Steady-state brake torque increases with increasing current and is a function of displacement. At large position oscillation amplitudes coulomb friction is a good approximation of the brakes torque response and energy dissipation. However, closer examination of the measured brake torque vs. position relationship, Fig. 3, shows a more continuous transition in torque during velocity reversal conditions. Our experiments show the brake is able to store energy and under small deflections and can behave more like a spring than a purely dissipative system.

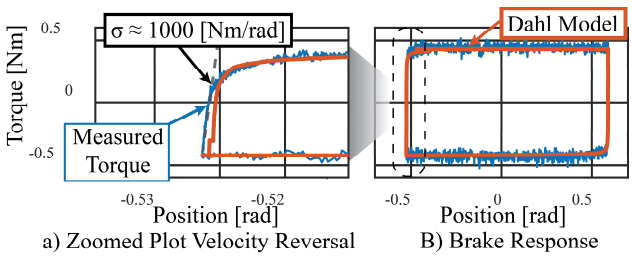

Figure 3. Measured torque response of the particle brake under constant current conditions and a position input a) Zoomed plot of the brake response showing a Dahl like response. B) Full position oscillation cycle and resulting brake torque response.

This behavior is akin to structural damping observed in bolted joints [18] and bearing friction. Taking inspiration from these sources we developed a modified Dahl friction model to describe the torque production and mechanical hysteresis of our brake under velocity reversal conditions [19]. A graphical comparison to measured brake torque and rotor position data can be seen in Fig. 3.

In addition to mechanical behavior, particle brake electrical dynamics, limit the change of current in the coil and influence torque production in the brake. Particle brakes also display a nonlinear and hysteretic relationship between current flowing in the coil and steady state output torque. The complete brake mathematical model is described in detail in Appendix A.

B. *Model-Based Passive Partitioning*

Our passive partitioning method, shown in Fig. 1 and 5, utilizes our particle brake model to estimate particle brake torque. Both electrical dynamics and mechanical hysteresis effects are important to produce a useful estimate of brake torque production. The torque command and brake position are the inputs to the brake dynamic model whereas the estimated brake torque is the model's output. If the open loop brake torque estimate is of the same sign as the commanded torque, indicating that the commanded torque is physically feasible given the brake's current state, then the commanded torque is sent to the brake. This approach removes brake commands which are not physically possible and if not removed would oppose the torque command.

Our method of partitioning the actuators commanded torque has several advantages over methods assuming purely dissipative passive actuator torques. First, power based partitioning methods have problems at zero or near zero velocity. In discrete systems with finite velocity resolution power-based partitioning can produce rapid switching at or near the sample frequency of the discrete time controller. This can cause chattering in the passive actuators rendered torque and affect the rendering of a haptic device without other mechanical or software provisions [13,15]. Passive torque commands obtained with our open loop model do not display the same switching behavior, as seen in Fig. 4. Additionally, the passive actuator is able to produce zero velocity passive torque. Finally, our passive partitioning method accounts for strain energy stored in the brake. Accounting for this has distinct advantages while the hybrid device is operating at high stiffness where energy stored in the brake plays a significant role in the dynamics of the device.

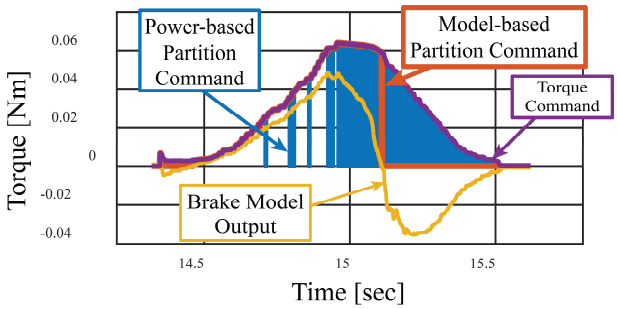

Figure 4. Time domain plot of the torque command by our model-based passive partitioning method compared to results obtained by power-based partitioning. The figure also shows the time domain results of the Dahl inspired model.

C. *Stiffness-Based Partitioning*

At high stiffness our torque partitioning method works well and the three goals for our hybrid control system are achieved. We attribute this to the behavior of the particle brake at small deflections. Our partitioning approach allows the brake to behave like a physical spring in parallel with the active actuator.

However, large position oscillation amplitudes are often encountered at low stiffness and the hybrid actuator begins to display undesirable "sticky wall" effects. Active actuators like the DC motor comprising half of our hybrid actuator are capable low stiffness actuators. Consequently, we choose to utilize only the active portion of our hybrid actuator while rendering low stiffness. Utilizing the active actuator at low stiffness prevents particle brake sticking. Our control structure, enabling a smooth transition between active only and hybrid operation, can be seen in Fig 5. In practice we set hybrid transition points from low stiffness active-only rendering to high stiffness hybrid rendering at a stiffness where sticky walls are no longer observed (20-21 [N/mm]). In most haptic applications the rendered stiffness is known and could be supplied as part of the control algorithm. However, in applications where the virtual environment stiffness is not known apriori an online estimation approach can be adopted (see Appendix B)

II. Mechanical Design

To evaluate our hybrid actuation and control approach we have developed a one-degree-of-freedom handheld prototype (see Fig. 6). The mechanical design of our handheld hybrid actuator seeks to achieve a high level of transparency with simple lightweight design. We achieve transparency with low inertia actuation and a stiff, efficient, low reduction, (9.3:1), cable transmission. Our control structure allows passive and active actuators to be rigidly linked together simplifying our mechanical design compared to other hybrid actuation approaches which require multiple brakes and overrunning clutches [15], mechanical differentials [16] and series elastic elements to function [12] while still producing zero velocity passive torque.

Our hybrid actuator utilizes a particle brake (Placid Industries B1) and a high-performance DC servo motor (Maxon DCX 22 S Ø22 mm with RIO 16 encoder 65536 CPT) connected in parallel. The device is capable of grasping and touching haptic interactions as shown in Fig. 6. An ATI Nano43 sensor provides brake torque feedback. The particle brake rotor itself has low inertia; and when the coil is unpowered only a small amount of latent friction remains. These properties make it an ideal choice as a low impedance passive actuator. An ironless core Maxon DC motor was selected as the active actuator to eliminate cogging torque and minimize rotor inertia. Cable transmissions, like the one used here, are very efficient and are nearly lossless. The low and efficient reduction prevents excessive reflected inertia at the output of the transmission helping the device to remain transparent.

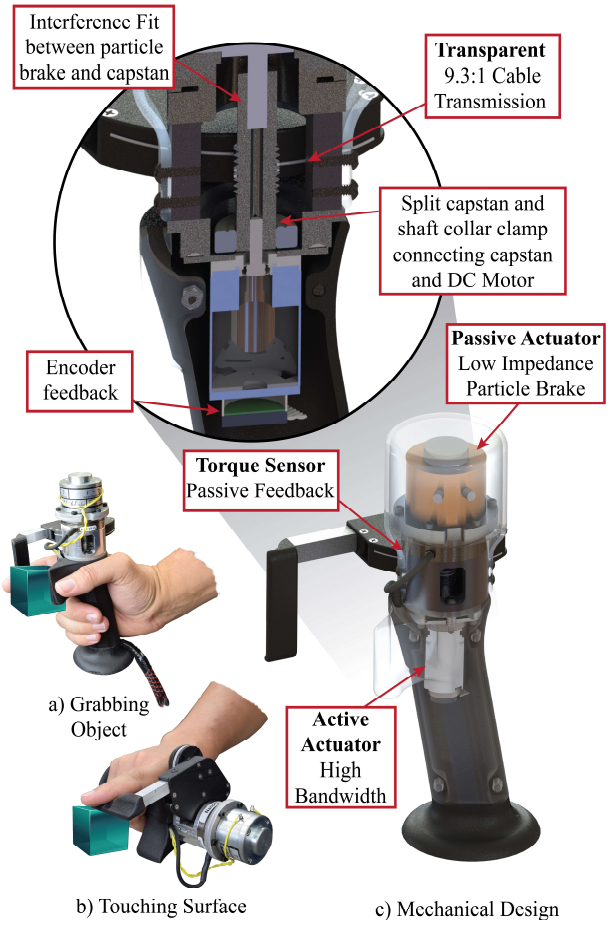

Figure 6. Two haptic interactions enabled by the handheld haptic device. a) Grabbing a virtual object b) Touching a surface. c) Low impedance mechanical design of the hybrid actuator enabling a transparent rendering.

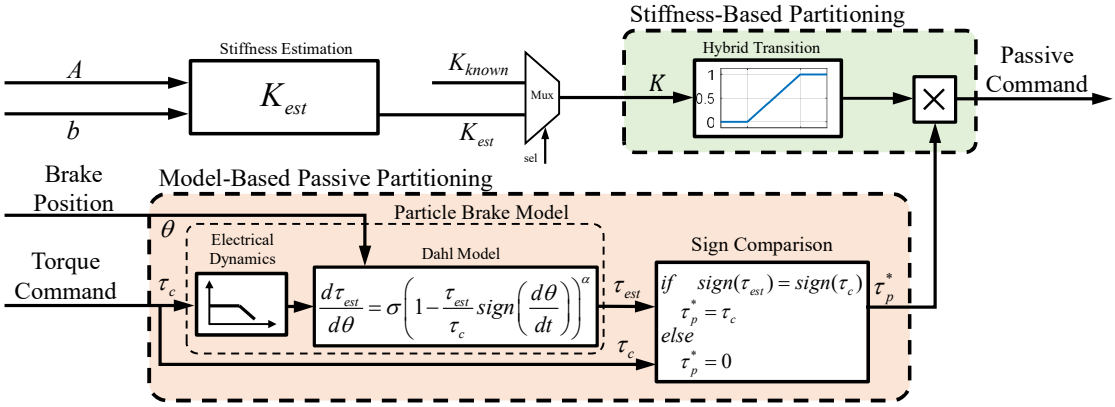

Figure 5. Passive partition including stiffness-based partitioning and model-based passive partitioning. Either a known or estimated stiffness might be used as the input signal for the hybrid transition. Additional information about the stiffness estimation method can be found in appendix B.

III. Experimental Evaluation

To evaluate the performance of our one-degree-of-freedom prototype, we conducted experiments to determine (1) the maximum rendering force and stiffness, (2) the kinesthetic rendering bandwidth (i.e. range of frequencies over which the prototype can accurately render kinesthetic forces with minimal amplitude and phase distortion) , and (3) latent friction forces to assess transparency. Finally, we programmed the device to display the force profile of a button to demonstrate how the dynamic range enabled through our control approach translates to common kinesthetic handheld haptic interactions.

A. Maximum Rendering Force and Stiffness

Providing larger forces and more importantly a larger range of impedances is the main motivation for the use of our hybrid actuation approach in place of typical active only actuation approaches. The Z-width, or range of stable impedances, has been traditionally used to evaluate the performance of a haptic device [20]. Specifically, the maximum stable virtual wall stiffness of a haptic device, one axis of a Z-width plot, is often used to evaluate the performance of an impedance based haptic device. To measure the maximum stable virtual wall stiffness the prototype was programed to render a unilateral virtual wall with various stiffness. The interaction was deemed to be stable if no discernable vibrations were present. The position domain plot of a representative stable interaction with the maximum virtual stiffness is shown in Fig. 7a. Data shown in Fig. 7 was captured using the grabbing grip shown in Fig. 6a.

Time domain data shown in Fig. 7 confirms the device is producing large forces. The device can render symmetrically below 10 [N] and asymmetrically, combining active and passive torque, to greater than 20 [N]. This assumes a three and one half inch moment arm to the point of finger contact. While rendering common haptic features, like a virtual wall, much of the steady state torque can be supplied passively. The active actuator can intermittently supply active torques of a similar magnitude as the passive actuator and the hybrid actuator functions well in many circumstances without the need for an active actuator sized for steady state torques. Furthermore, the maximum stiffness of the hybrid device (60 [N/mm]) is stiffer than the maximum achievable stiffness from the active device alone (30 [N/mm]). Our hybrid control system improves the achievable range of forces and stable stiffness as compared to typical active only impedance based haptic devices without compromising the haptic rendering.

B. Kinesthetic Rendering Bandwidth

The virtual wall experiments show our device accurately captures the user's kinesthetic motions. However, researchers have found that the realism of a kinesthetic haptic interaction is influenced by high frequency transients and that the display of faster force transients is vital to stimulating the user perception [21]. Consequently, the range of frequencies a kinesthetic haptic device can render, referred to here as its rendering bandwidth, is important to haptic interactions.

To assess the rendering bandwidth of our prototype we constructed an experimental testbed to measure the output impedance of the prototype over a range of frequencies. Our test setup consists of a voice coil actuator (Kimco LA12-17-000A) and the hybrid haptic device. A load cell (TAL2205) is mounted on the hybrid haptic device to measure the interaction forces between the voice coil and device. A linkage connects the voice coil actuator to the haptic device through the load cell.

In our experiments, the device was programmed to render a pure spring. Interaction forces were varied through activation of the voice coil actuator (i.e. a chirp signal from 0.1 to 100 [Hz] frequency, applied over 10 cycles lasting 10 seconds each). Impedance measurements obtained from these tests, Fig. 8, shows a rendering bandwidth from a virtual spring, (60 [N/mm]), up to at least 100 [Hz] with minimal magnitude or phase distortion. At smaller stiffness, 0.6 and 6 [N/mm], the mass of the device itself causes the high frequency asymptote observed in the magnitude plot and the corresponding gain in phase. Despite the distortion, the virtual spring is still producing torque at higher frequencies and the rendering bandwidth remains unchanged. We can conclude that our hybrid haptic device is able to capture user motions and accurately render kinesthetic forces across a broad frequency range, at least to 100 [Hz], important to the realism of haptic interactions.

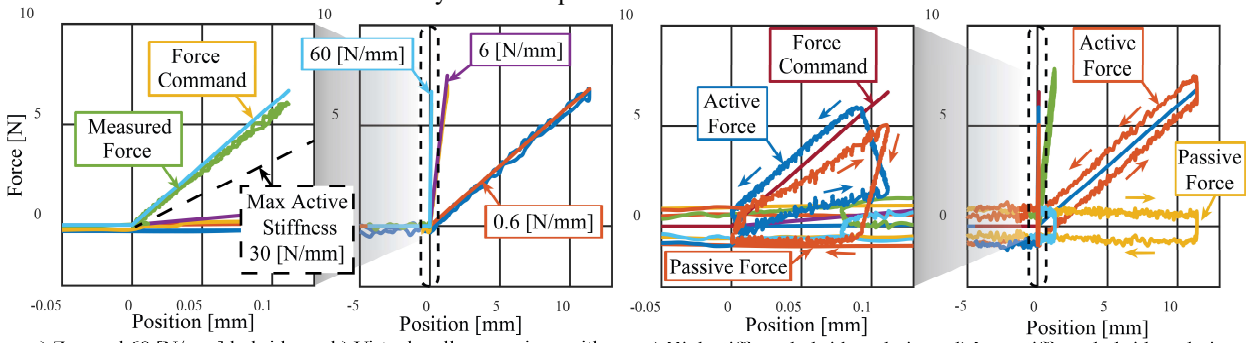

a) Zoomed 60 [N/mm] hybrid command and measured force
b) Virtual wall comparison with active only and hybrid rendering
c) High stiffness hybrid rendering with active and passive torques
d) Low stiffness hybrid rendering with active and passive torques

Figure 7. Maximum coupled stable stiffness 60 [N/mm] and two lower stiffness 6 [N/mm] and 0.6 [n/mm] left to right respectively. The sample frequency is set at 5000 [Hz] for all tests. a) Zoomed plot of maximum stiffness. b) Virtual wall comparison. c) Active and passive contributions to the stiffest stable virtual wall. d) Virtual wall comparison showing active command and measured passive torque contributions at lower stiffness.

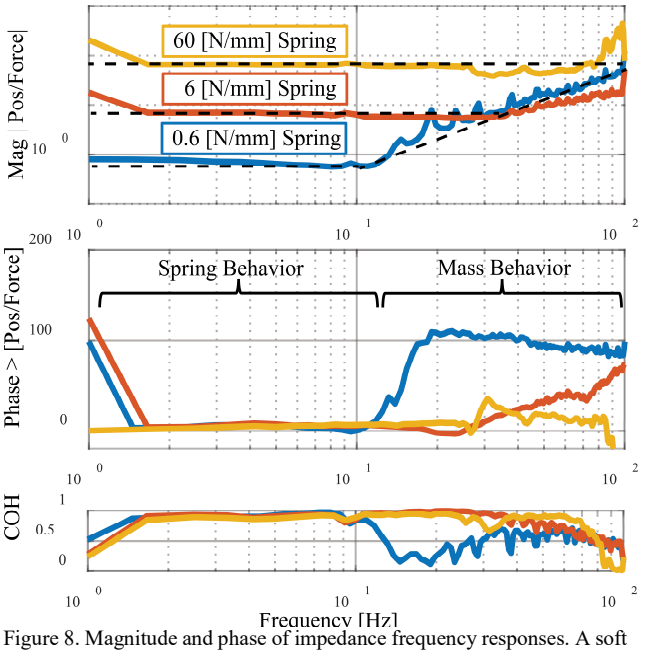

Figure 8. Magnitude and phase of impedance frequency responses. A soft (0.6 [N/mm]), medium (6 [N/mm]), and stiff (60 [N/mm]), spring are shown in blue red and yellow respectively. A chirp is used to excite the system from 0.1 [Hz] to 100 [Hz]. A Hanning window, 50% overlap, and 199 frequency averages we taken [Hz] and the discrete control system is running at 5000 [Hz]

C. *Latent Friction / Transparency*

Impedance-based devices are designed to have low reflected inertia and drive-train friction to achieve a transparent feeling. To assess transparency, the device was programmed for an impedance of zero (i.e. no force as a function of position). Users interacted with the device and output forces were measured using a load cell at the end of the device finger rest. Fig. 9 shows transparency measurements of the device in free space. The device displays a minimal amount of friction, 0.06 – 0.15 [N] on average over the measured intervals, while under normal operation.

Low measured friction and resulting transparency results from both the low mechanical impedance of the prototype's design and the proposed control approach which incorporates direct feedback of the brake's output torque. Our control system measures latent particle brake friction and masks it with the active actuator. It is worth noting that transparency is only improved within the bandwidth of passive torque feedback. When moving in one direction the filtered latent friction measurement is nearly exact and almost no resistive force can be felt. Transparency is only compromised when the direction of motion changes and latent friction forces are generated beyond the bandwidth of passive torque feedback.

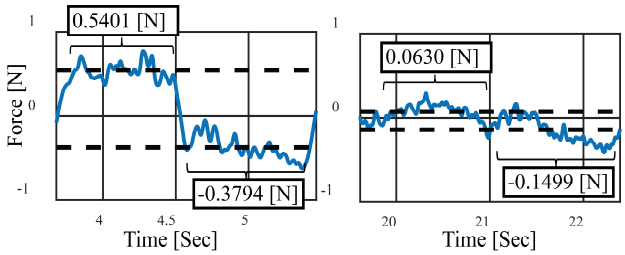

a) Measured Output - No Control b) Measured Force - Hybrid Control

Figure 9. Filtered measured output torque (5 [Hz] B.W. Zero Lag SOF) at the output of the handheld haptic device while a) the device is off and b) while the control system is compensating for latent particle brake torque. Average torque over each bracketed interval is shown in boxes.

A. *Complex Button Force Profile*

A button is a common haptic effect that demonstrates the capabilities of the hybrid handheld haptic device. Buttons have a stiff nonlinear and sometimes hysteretic force deflection profiles. To qualitatively assess the performance of our control approach we programmed our prototype to render a button force profile. We use the button model in [22] to create the force deflection profile of a common pushbutton. Fig. 10 shows the force deflection profile resulting from the button model.

Accurately rendering the button displays the handheld hybrid haptic devices dynamic range and ability to render features of an immersive virtual environment. The hybrid control system transitions between active only rendering and hybrid rendering when stiffness increases and can render both soft and stiff environments. The characteristic button click requires an actuator with all the components of dynamic range to render convincingly. Table two summarizes our experimental results characterizing the dynamic range of the hybrid handheld haptic device and compares them to existing devices.

TABLE II. COMPARISON OF HANDHELD AND WEARABLE KINESTHETIC HAPTIC DEVICES

		Handheld Kinesthetic Haptic Device Design Criteria				
Device		***Large Forces***	***Large Bandwidth of Force***	***Transparent ~Friction Force***	***Largest Stable Stiffness***	***Mass*****
Passive And Shape Rendering	Wolverine [2]	105 [N]	--	--	162 [N/mm]	55 [g]
	MR Glove [1]	0.821 [Nm]	--	0.005 [Nm]	--	640 [g]
Admitance Devices	CLAW [3]	30 [N]	--	0.5N	5.73 [N/mm]	420 [g]
SEA Devices	Maestro Hand Exoskeleton [5]	16 [N]	10 [Hz]	--	--	136 [g]
	SEA Hand Exoskeleton [6]	9 [N]	--	--	--	298 [g]
DC motors with speed reducers	Geared DC Motor [7]	0.363 [Nm]	--	--	--	--
	Cybergrasp [8]	12 [N]	40 [hz]	--	--	539 [g]
Pnumatic Actuation	Rutgars Haptic Master II [8]	16 [N]	10 [Hz]	0.014 [N]	--	80 [g]
	Soft Actuator Glove [9]	2.1 [N]	--	0.58 [N]	--	30.8 [g
Hybrid Actuators	Hybrid Handheld Device	10-20* [N]	>100 [Hz]	0.06-0.15 [N]	60 [N/mm]	550 [g]

*10 newtons is the symetric rendering range of the device. 20 newtons of force can be achieved by summing active and passive forces. Generated forces were measured at a 3.5" moment arm. **The mass column comparison uses the mass at the users hand. If actuators were located away from the hand acuator mass was not included.

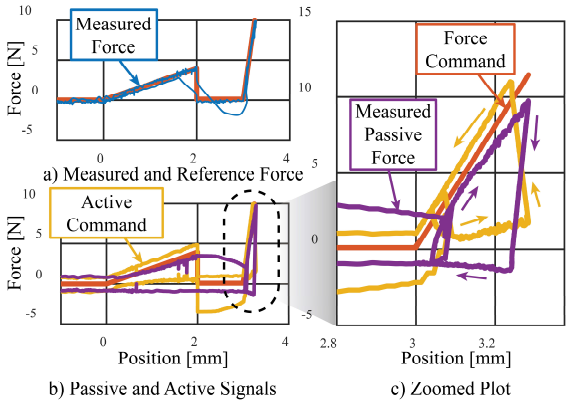

Figure 10. Hybrid rendering of a button K1 = 2N/mm Fr = 0.1 K2 = 40N/mm m = 2mm n = 3mm fs = 5000 [Hz] a) Compares measured Zero Lag Filtered (SOF 40Hz cutoff) output force (blue) and Reference torque (red) b) Shows the reference torque (red) and the measured filtered passive force (purple and the commanded active torque (yellow) c) Is a zoomed plot of the stiff wall interaction at the end of the buttons throw.

Table two shows our hybrid device excels in the bandwidth of force provided and the range of virtual stiffness it can achieve. The maximum forces obtained by the device are of comparable magnitude to most existing actuation approaches. Hybrid actuator transparency is not linked to a minimum mass as it is in admittance controlled devices and measured friction is of a similar maximum magnitude but often much less than other actuation approaches. Our prototype is heavier than many handheld devices, but all actuators are located in the device as opposed to the cable driven designs used in Maestro [5] and CyberGrasp [13].

IV. Conclusion and Future Work

Our hybrid control approach brings dynamic range needed to render diverse virtual environments to the handheld form factor. Our hybrid control system does so though the use of a novel particle brake model, partitioning system, and torque feedback. The actuation and control approach enables increased dynamic range and eliminates common hybrid rendering artifacts like the "sticky wall". Our control approach enables simple mechanical design necessary for handheld haptic applications. The prototype device compares favorably to existing devices in performance but could be considered heavy for a handheld device.

The prototype hybrid handheld device presented here only contains one degree of freedom and weighs 550 grams. Integrating the passive torque sensor more fully into the structure of the actuator by using bonded strain gauges would simplify design further, stiffen the device, and reduce weight. Additional design iterations could significantly reduce the weight and size. Testing the hybrid actuation approach on a multiple degree of freedom platform remains a subject of future work. Finally, we wish to explore the rendering accuracy and bandwidth for other haptic impedance effects in addition to the pure stiffness discussed here.

Acknowledgment

This work was made possible, in part, through funding from the National Science Foundation granted to co-authors Dills and Zinn in their academic rolls at the University of Wisconsin-Madison. (grant: NSF 1830516)

Appendix A – Particle Brake Dynamics

The particle brake has linear and nonlinear characteristics as mentioned in the particle brake dynamics section. The block diagram shown in Fig 11. Summarizes how our brake model – –is applied.

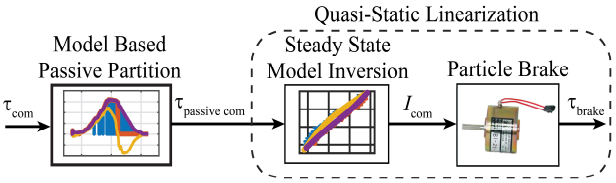

Figure 11. Block diagram showing quasi-static model inversion to improve steady state torque rendering accuracy, and the model based passive partition which includes electrical and mechanical dynamics.

A. Quasi-Static Torque Current Model Inversion

A nonlinear and hysteretic relationship exists between the current flowing in the brakes coil and the steady state output torque of the brake as shown in Fig. 12a. To model this relationship and increase the accuracy of the brakes steady state output torque we utilize a model inverse solution. Inverting the steady state or quasi-static torque to current relationship and fitting third order polynomials to the rising and falling curves forms the boundary of the rate independent hysteretic relationship. We utilize a rate independent hysteresis model of the Dahl variety to transition back in forth between the two fitted curves forming minor loops, Fig. 12.

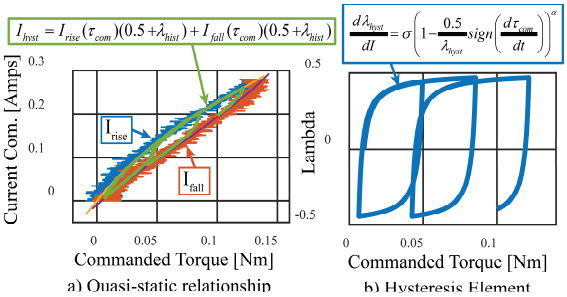

Figure 12 a) Quasi-static steady state torque current relationship. With third order polynomials I1 and I2 b) Hysteresis element (lambda) forming minor loops of rate independent hysteresis behavior.

B. Velocity Reversal Dynamics – Mechanical Hysteresis

As stated in the particle brake dynamics section we use a modified Dahl friction model, (1), to model mechanical hysteresis observed in the brake.

$$\frac{d\tau_b}{d\theta_b} = \sigma\left(1 - \frac{\tau_c}{\tau_b}\, sign\left(\frac{d\theta_b}{dt}\right)\right)^{\alpha} \qquad (1)$$

Where:

σ = Brake Stiffness
α = Hysteresis shape parameter
τ_b = Brake torque
θ_b = Brake rotor position
τ_c = The coulomb or steady state brake torque

The modified Dahl model utilizes the output of our electrical dynamic model to change the steady state brake torque. Our quasi-static model inversion makes this possible by linearizing steady state torque characteristics of the brake.

C. Electrical Dynamic Model

Electrical dynamics of the brake give it low pass characteristics. The brake amplifier (Copley JSP-090-10) utilizes a PI current controller. Resistance and inductance

associated with the brakes coil limits the rate of change of current and steady state torque production. A closed loop transfer function describing the command tracking current response of a linear inductive load may be written in the form of (2) and is used to represent electrical dynamics of the brake.

$$\frac{\tau(s)}{\tau^*(s)} = \frac{I(s)}{I^*(s)} = \frac{K_p s + K_i}{Ls^2 + \left(R + K_p\right)s + K_i} \qquad (2)$$

Appendix B – Online Impedance Estimation

A more general stiffness estimation approach might be necessary for applications in nonlinear or telerobotic environments where the stiffness of the rendered impedance is unknown. In this case we adopt a method for online parameter estimation. One method we have found useful to estimate the linear stiffness of an unknown virtual environment is the restoring force surface method (3) and [23].

$$\begin{aligned} K_{est} &= \left(A^T A\right)^{-1} A^T b \\ A &= \begin{bmatrix} \theta_k & \theta_{k-1} & \theta_{k-2} & \dots & \theta_{k-n} \end{bmatrix} \\ b &= \begin{bmatrix} \tau_k & \tau_{k-2} & \tau_{k-2} & \dots & \tau_{k-n} \end{bmatrix} \end{aligned} \qquad (3)$$

Where:

K_{est} = The estimated stiffness at the current sample instant

θ = The measured position error of the actuator at sample k.

τ = The torque commanded to the actuator at sample k.

Incorporating an online impedance estimation method into our control algorithm makes it suitable for the most general circumstances encountered by a haptic device.

References

[1] Blake, J., and H.B. Gurocak. "Haptic Glove With MR Brakes for Virtual Reality." IEEE/ASME Transactions on Mechatronics 14, no. 5 (October 2009): 606–15. https://doi.org/10.1109/TMECH.2008.2010934.

[2] Choi, Inrak, Elliot W. Hawkes, David L. Christensen, Christopher J. Ploch, and Sean Follmer. "Wolverine: A Wearable Haptic Interface for Grasping in Virtual Reality." In 2016 IEEE/RSJ International Conference on Intelligent Robots and Systems (IROS), 986–93. Daejeon, South Korea: IEEE, 2016. https://doi.org/10.1109/IROS.2016.7759169.

[3] Choi, Inrak, Eyal Ofek, Hrvoje Benko, Mike Sinclair, and Christian Holz. "CLAW: A Multifunctional Handheld Haptic Controller for Grasping, Touching, and Triggering in Virtual Reality." In Proceedings of the 2018 CHI Conference on Human Factors in Computing Systems - CHI '18, 1–13. Montreal QC, Canada: ACM Press, 2018. https://doi.org/10.1145/3173574.3174228.

[4] G. A. Pratt and M. M. Williamson, "Series elastic actuators," Proceedings 1995 IEEE/RSJ International Conference on Intelligent Robots and Systems. Human Robot Interaction and Cooperative Robots, Pittsburgh, PA, USA, 1995, pp. 399-406 vol.1. https://doi: 10.1109/IROS.1995.525827

[5] Agarwal, Priyanshu, Youngmok Yun, Jonas Fox, Kaci Madden, and Ashish D Deshpande. "Design, Control, and Testing of a Thumb Exoskeleton with Series Elastic Actuation." The International Journal of Robotics Research 36, no. 3 (March 2017): 355–75. https://doi.org/10.1177/0278364917694428.

[6] Jo, Inseong, and Joonbum Bae. "Design and Control of a Wearable Hand Exoskeleton with Force-Controllable and Compact Actuator Modules." In 2015 IEEE International Conference on Robotics and Automation (ICRA), 5596–5601. Seattle, WA, USA: IEEE, 2015. https://doi.org/10.1109/ICRA.2015.7139982.

[7] Pierce, Rebecca M., Elizabeth A. Fedalei, and Katherine J. Kuchenbecker. "A Wearable Device for Controlling a Robot Gripper with Fingertip Contact, Pressure, Vibrotactile, and Grip Force Feedback." In 2014 IEEE Haptics Symposium (HAPTICS), 19–25. Houston, TX, USA: IEEE, 2014. https://doi.org/10.1109/HAPTICS.2014.6775428.

[8] Bouzit, M., G. Burdea, G. Popescu, and R. Boian. "The Rutgers Master II-New Design Force-Feedback Glove." IEEE/ASME Transactions on Mechatronics 7, no. 2 (June 2002): 256–63. https://doi.org/10.1109/TMECH.2002.1011262.

[9] Zhang, Yu, Dangxiao Wang, Ziqi Wang, Yueping Wang, Li Wen, and Yuru Zhang. "A Two-Fingered Force Feedback Glove Using Soft Actuators." In 2018 IEEE Haptics Symposium (HAPTICS), 186–91. San Francisco, CA: IEEE, 2018. https://doi.org/10.1109/HAPTICS.2018.8357174.

[10] An, Jinung, and Dong-Soo Kwon. "Stability and Performance of Haptic Interfaces with Active/Passive Actuators—Theory and Experiments." The International Journal of Robotics Research 25, no. 11 (November 2006): 1121–36. https://doi.org/10.1177/0278364906071034.

[11] Rossa, Carlos. "A hybrid actuation system for haptic interfaces," 2013. https://doi.org/10.13140/2.1.4028.7367.

[12] Conti, François, and Oussama Khatib. "A New Actuation Approach for Haptic Interface Design." The International Journal of Robotics Research 28, no. 6 (June 2009): 834–48. https://doi.org/10.1177/0278364908097958.

[13] Jinung An, and Dong-Soo Kwon. "Five-Bar Linkage Haptic Device with DC Motors and MR Brakes." Journal of Intelligent Material Systems and Structures 20, no. 1 (January 2009): 97–107. https://doi.org/10.1177/1045389X07086690.

[14] Antolini, Michele, Orhun Kose, and Hakan Gurocak. "A First Order Transfer Function to Balance the Workload in Brake-Motor Hybrid Actuators." In 2014 IEEE Haptics Symposium (HAPTICS), 509–14. Houston, TX, USA: IEEE, 2014. https://doi.org/10.1109/HAPTICS.2014.6775508.

[15] Rossa, Carlos, Jose Lozada, and Alain Micaelli. "Design and Control of a Dual Unidirectional Brake Hybrid Actuation System for Haptic Devices." IEEE Transactions on Haptics 7, no. 4 (October 1, 2014): 442–53. https://doi.org/10.1109/TOH.2014.2346501.

[16] Chapuis, Dominique, Xavier Michel, Roger Gassert, Chee-Meng Chew, Etienne Burdet, and Hannes Bleuler. "A Haptic Knob with a Hybrid Ultrasonic Motor and Powder Clutch Actuator." In Second Joint EuroHaptics Conference and Symposium on Haptic Interfaces for Virtual Environment and Teleoperator Systems (WHC'07), 200–205. Tsukuba, Japan: IEEE, 2007. https://doi.org/10.1109/WHC.2007.5.

[17] Gosline, Andrew H. C., and Vincent Hayward. "Eddy Current Brakes for Haptic Interfaces: Design, Identification, and Control." IEEE/ASME Transactions on Mechatronics 13, no. 6 (December 2008): 669–77. https://doi.org/10.1109/TMECH.2008.2004623.

[18] Deaner, Brandon J., Matthew S. Allen, Michael J. Starr, and Daniel J. Segalman. "Investigation of Modal Iwan Models for Structures with Bolted Joints." In Topics in Experimental Dynamic Substructuring, Volume 2, edited by Randy Mayes, Daniel Rixen, and Matt Allen, 9–25. New York, NY: Springer New York, 2014. https://doi.org/10.1007/978-1-4614-6540-9_2.

[19] Dahl, Philip R. "Solid Friction Damping of Mechanical Vibrations." AIAA Journal 14, no. 12 (December 1, 1976): 1675–82. https://doi.org/10.2514/3.61511.

[20] Colgate, J.E., and J.M. Brown. "Factors Affecting the Z-Width of a Haptic Display." In Proceedings of the 1994 IEEE International Conference on Robotics and Automation, 3205–10. San Diego, CA, USA: IEEE Comput. Soc. Press, 1994. https://doi.org/10.1109/ROBOT.1994.351077.

[21] Kuchenbecker, K.J., J. Fiene, and G. Niemeyer. "Improving Contact Realism through Event-Based Haptic Feedback." IEEE Transactions on Visualization and Computer Graphics 12, no. 2 (March 2006): 219–30. https://doi.org/10.1109/TVCG.2006.32.

[22] Burdea, Grigore. Force and Touch Feedback for Virtual Reality. New York : John Wiley & Sons, [1996] ©1996, 1996. https://search.library.wisc.edu/catalog/999793349902121

[23] Allen, Matthew S., Hartono Sumali, and David S. Epp. "Piecewise-Linear Restoring Force Surfaces for Semi-Nonparametric Identification of Nonlinear Systems." Nonlinear Dynamics 54, no. 1–2 (October 2008): 123–35. https://doi.org/10.1007/s11071-007-9254-x.